14th International Symposium on Turbulence and Shear Flow Phenomena (TSFP14)
Heidelberg, Germany, July 28–31, 2026

HOW DO THREE-DIMENSIONAL WAKE PATTERNS AFFECT FORCES ON TRAPEZOIDAL FLAGS?

Agathe Schmider
Mechanical Engineering
EPFL
Lausanne, Switzerland
agathe.schmider@epfl.ch

Gaétan Raynaud
Mechanical Engineering
EPFL
Lausanne, Switzerland
gaetan.raynaud@epfl.ch

Karen Mulleners
Mechanical Engineering
EPFL
Lausanne, Switzerland
karen.mullener@epfl.ch

ABSTRACT

This study investigates the influence of tapering on the flapping dynamics and wake topology of flexible flags in a uniform flow. Tapering in trapezoidal flags comes from the variation of height along the flag, with converging flags leaning towards triangles and diverging flags resembling simplified fishtails. The degree and direction of tapering affects the flapping kinematics and dynamics. The mean drag coefficient of diverging flags is almost double the one of converging flags. Two-dimensional particle image velocimetry in the mid-plane reveals differences in the transverse extent of the wake and the structure of the shear layer. The amount of vorticity and the velocity deficit in the midplane section are not sufficient indicators to explain the difference in total drag. Future work involves scanning stereo-PIV in multiple cross-section planes to reconstruct the three-dimensional topology of the vortical structures in the wake of trapezoidal flags. The goal is to use the experimental data to adapt a quasi-steady aerodynamic model based on Prandtl's lifting line approach to predict forces on flapping flags with different taper ratios.

INTRODUCTION

Fish rely on the oscillation of their flexible tails to generate thrust by shedding vortices in the wake. The topology of the wake vortices are inherently three-dimensional. A purely two-dimensional description, for instance from mid-plane measurements, can be a misleading indicator of swimming performances, as the complex vortex structures that govern thrust generation are inherently three-dimensional (Floryan *et al.*, 2020). Specifically, the planform shape of the propulsive surface directly influences the three-dimensional vortex topologies, which in turn affect the fluid loading. Actively pitched panels of different aspect ratio and edge geometries generate various vortex topologies and thrust production (King & Green, 2023). Higher circulation is observed for forked panels compared to pointed panels without a benefit on thrust production. To systematically investigate the link between the shape of an aerodynamic object, wake topology, and loading, we focus here on the passive fluid-structure interactions of flapping flags.

Flags are pieces of flexible materials immersed in a flow. Beyond a critical velocity, the flag undergoes large-amplitude periodic flapping, which generates a characteristic shear layer and vortex street in the wake. By changing the taper ratio of trapezoidal flags, we induce changes in the spanwise loading and modulate the fluid forces experienced by the flag. The tapering is a key parameter that influences the onset of flapping (Pang *et al.*, 2010) and the post-critical dynamics. This study uses the flapping flag as a model to bridge the gap between complex three-dimensional wake topology and the measured forces.

EXPERIMENTAL APPROACH

We focus on the differences of flapping dynamics and wake topology between rectangular and trapezoidal flags during the post-critical flapping regime. Systematic tests with flags made out of paper are conducted in an open-section wind tunnel (fig. 1a). Time-resolved measurements of the centreline deformation are obtained with an event-based camera for a range of flow velocities (Raynaud & Mulleners, 2025). The flags are cut out of paper, with a constant length L and constant area $S = L(H_0 + H_1)/2$, where H_0 and H_1 are the heights at the root and tip. Variations of tapering are quantified by the taper ratio H_1/H_0. Here, we change the taper ratio from 0 to 2.33. Flags with a low taper ratio have a converging geometry. Flags with a high taper ratio have a diverging geometry. We performed planar particle imaging velocimetry (PIV) in the mid-plane. The PIV data are phase-averaged and the phase of each snapshot is obtained based on the first two POD mode coefficients. Force measurements are gathered with strain gauges mounted on the flag pole platform. The mean drag value is time-averaged over the duration of the recording for a given flow velocity. The evolution of the mean drag value and the flapping kinematics with flow velocity is tested by increasing the flow velocity successively between recordings.

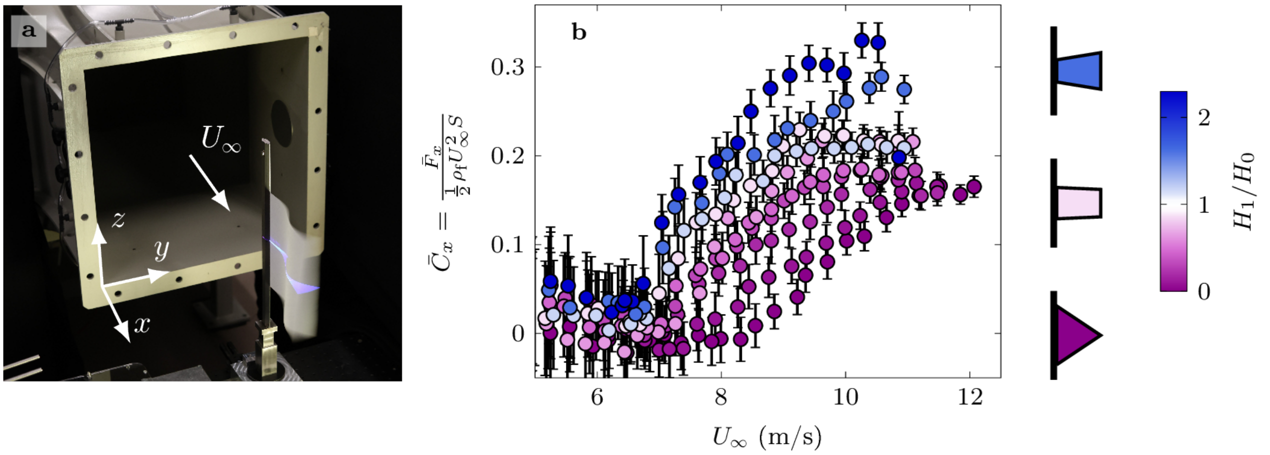

Figure 1. (a) Experimental set up. The deformed centreline is lit up in blue. (b) Evolution of the mean drag coefficient $\overline{C}_x$ for flags with different taper ratios.

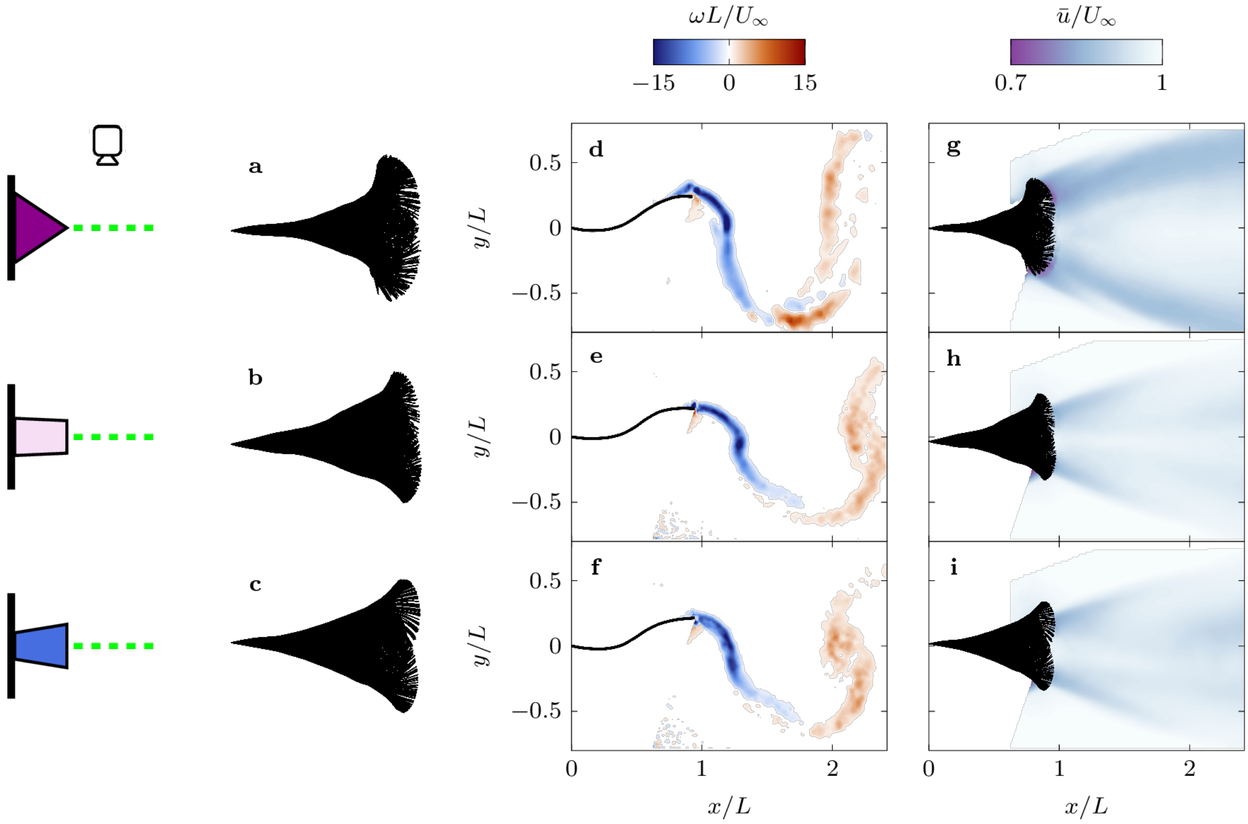

Figure 2. (a-c) Flapping envelopes, (d-f) phase-averaged snapshots of dimensionless vorticity $\omega L/U_\infty$ and time-averaged streamwise velocity component $\bar{u}/U_\infty$ measured at the midline of flags of increasing taper ratios (a, d, g) $H_1/H_0 = 0$, (b, e, h) $H_1/H_0 = 0.82$ and (c, f, i) $H_1/H_0 = 1.65$.

DYNAMICS OF TRAPEZOIDAL FLAGS

The mean drag coefficient $\overline{C}_x$ is obtained by normalising the dimensional drag force $\overline{F}_x$ with the dynamic pressure $\frac{1}{2}\rho_f U_\infty^2$ and the flag area $S = \frac{1}{2}L(H_0 + H_1)$:

$$\overline{C}_x = \frac{\overline{F}_x}{\frac{1}{2}\rho_f U_\infty^2 S}, \tag{1}$$

where ρ_f is the fluid density, U_∞ the incoming flow velocity and L the length of the flag at the midplane. For each flag, the mean drag coefficient is close to 0 before the onset of flapping, for $U_\infty < 7\,\mathrm{m\,s^{-1}} - 8\,\mathrm{m\,s^{-1}}$ depending on the flag (fig. 1b). The mean drag coefficient increases with flow velocity after the onset of flapping and reaches a plateau of maximum drag. The maximum value of the mean drag coefficient for each flag goes from $\overline{C}_x = 0.16$ to 0.33 when increasing the taper ratio from $H_1/H_0 = 0$ to 2.33. The flapping motion of diverging flag shapes extracts twice the amount of momentum from the flow compared to converging flag shapes.

To understand how the forces are connected to the flapping kinematics, we first analyse the mid-plane deformation measurements (fig. 2a-c). The mid-plane deformations re-

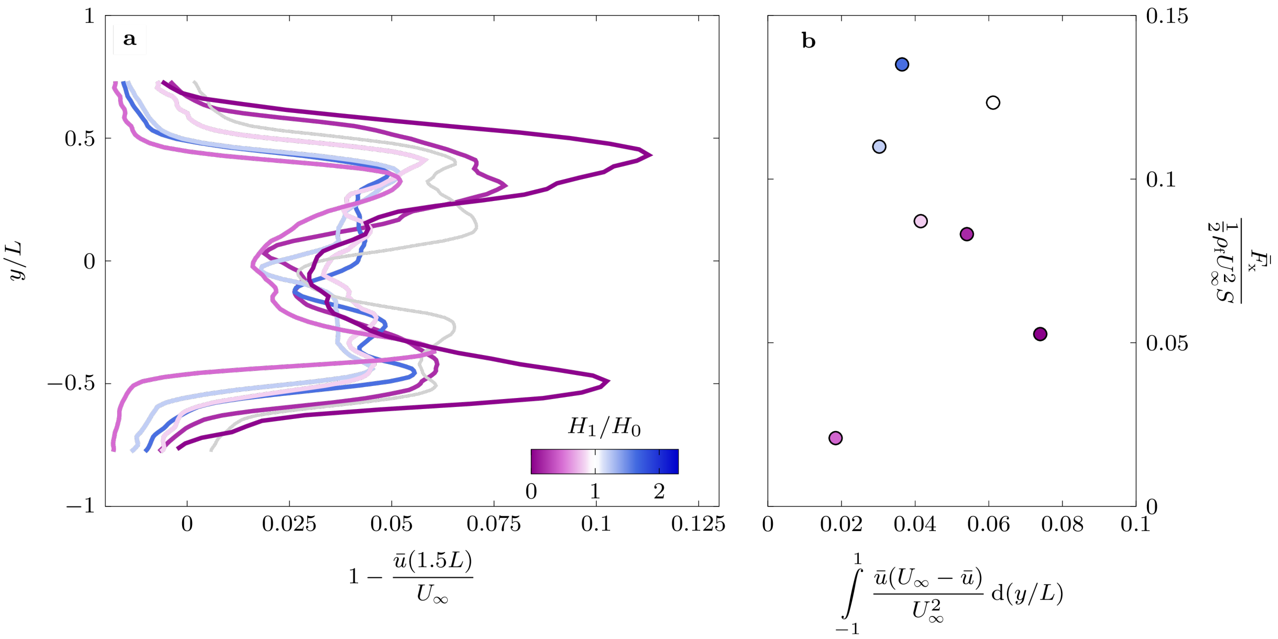

Figure 3. (a) Streamwise velocity deficit profiles at $x = 1.5L$ downstream of the root of the flag, (b) Comparison of the measured time-average drag coefficient $\bar{C}_x$ and the momentum deficit calculated at $x = 1.5L$ downstream of the root of the flag for flags of taper ratio $H_1/H_0 \in [0, 1.65]$

.

veal a node-less large-amplitude flapping for all tested flags. The absence of a node indicates that a travelling wave propagates along the centreline. The flapping envelope, obtained by stacking snapshots of the time-resolved deformations, indicates the spatial distribution of the flapping amplitude. Converging flag shapes have a lower flapping amplitude close to the root, and the flapping amplitude increases sharply towards the tip (fig. 2a). Diverging flag shapes have a larger amplitude in the middle section and the curvature of the centreline close to the tip is reduced (fig. 2c) compared to the converging flag (fig. 2a). Tapering alters the distribution of the bending stiffness along the flag (Leroy-Calatayud *et al.*, 2022). The converging flag is more rigid at the root leading to a reduced amplitude in the middle section. Its more pointy tip gives it more flexibility leading to a sharp increase in flapping amplitude and large curvature towards the tip. Due to the larger curvature at the tip of converging flags, we expect larger streamwise pressure gradients there. Pressure gradients are one of the main causes for vorticity generation along a surface (Terrington *et al.*, 2020). Less surface is available near the tip to generate vorticity for the converging flag and the reduction in effective surface competes against the higher vorticity production rate.

Snapshots of phase-averaged non-dimensionalised vorticity measured at the mid span are shown in fig. 2d-f for three flags of different tapering. The example snapshots for the different flags are extracted at the same phase in the flapping cycle. Vorticity accumulates along the surface of the flag and is released from the tip. The wake of the converging flag is widest. Its width is approximately $1.4L$ at $x/L = 1.5$ (fig. 2d,g). The wakes of the straight (fig. 2e,h) and diverging (fig. 2f,i) flags are comparable and reach a width of $\approx 1.1L$ at $x/L = 1.5$. The shear layer rolls up into a coherent vortex at $x \approx 1.2L$ in the wake of the straight flag (fig. 2e). The roll-up is less pronounced or even absent in the wakes of the diverging and converging flags. The strongest streamwise velocity deficit occurs for the converging flag (fig. 2g-i) despite having the lowest mean drag coefficient.

We analyse the average velocity deficit profiles at $x = 1.5L$ downstream of the flag (fig. 3a). The most converging flag $H_1/H_0 = 0$ has the highest velocity deficits, with two peaks around $[0.11 - 0.10]$ symmetrically distributed at $y/L = 0.49$ and $y/L = -0.43$. The average velocity deficit in the middle of the wake is lower, around $1 - \bar{u}/U_\infty = 0.03$. Flags with a converging shape all lead a similar "M" shaped velocity deficit profile in their wake. The maximum velocity deficit decreases with the taper ratio H_1/H_0. The velocity deficit in the middle of the wake is similar for all converging flags, between $1 - \bar{u}/U_\infty = [0.016 - 0.03]$. Flags with straight or diverging shapes have a flatter velocity deficit profile, with $1 - \bar{u}/U_\infty = [0.02 - 0.06]$ between $y/L = \pm 0.5$. The velocity deficits observed in the mid-plane wake are inconsistent with the measured drag coefficients. The highest drag coefficients are obtained for the diverging flags with high taper ratio, which should lead to the highest velocity deficit in the wake, due to more momentum transfer from the flow to the flapping flag. The higher velocity deficits in the mid-plane are observed for the most converging flags. We calculate the momentum deficit to systematically estimate the drag coefficient and compare it to the averaged force measurements to investigate this inconsistency. The momentum deficit is

$$I_{\text{def}} = \int_{y=-L}^{L} \frac{\bar{u}(x = 1.5L, y)(\bar{u} - U_\infty)}{U_\infty^2 L}\, \mathrm{d}y \quad . \tag{2}$$

In fig. 3b, we show measured drag coefficient $\overline{C}_x$ versus the momentum deficit calculated from the stream-wise velocity profiles at the flag mid-height. Consistently with the drag coefficients presented in fig. 1b, we observe the highest drag coefficients for diverging flags and the lowest drag coefficients for converging flags. The computed momentum deficit spans

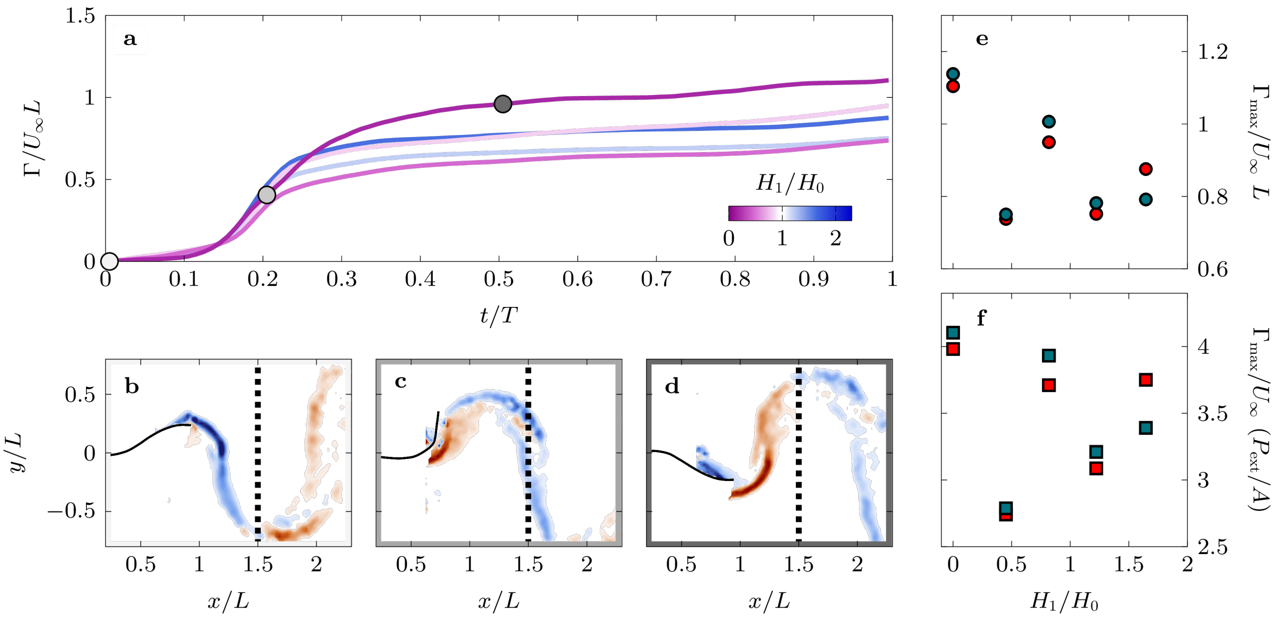

Figure 4. (a) Flux of negative circulation over a flapping cycle through the vertical line at $x = 1.5L$ downstream of the root of the flag normalised with the length L for flags of taper ratio $H_1/H_0 = 0 \in [0, 1.65]$. (b)-(d) Selected snapshots of the vorticity fields at different phases of the flapping cycle. (e)-(f) Maximum value of the positive (red) and negative (blue) circulation fluxes during a flapping cycle. (e) Normalisation with the maximum length L of the flags. (f) Normalisation with the ratio of the external perimeter to flag area.

a smaller range than the measured drag coefficient and does not show a clear dependence on the taper ratio. The momentum deficit from the velocity in the mid-plane is not a sufficient metric to characterise the drag force in the wake of flags with converging and diverging shapes. The discrepancy likely comes from two limitations of the mid-plane flow velocity measurements. First, the mid-plane profiles miss the three-dimensional structure of the wake. For a rectangular flag, the mid-height plane is representative of most of the span, so the momentum deficit measured in the mid-plane gives a reasonable estimation of the drag. For converging flags, the local chord length is shorter and the trailing-edge position is closer to the root when we move away from the midline. This would likely lead to a weaker momentum deficit that is estimated purely from the midplane measurements. For diverging flags, the spanwise variation in chord length and trailing-edge geometry would produce a tilted vortex tube which would stretch out of the midplane, so that a significant fraction of the streamwise momentum deficit is concentrated away from the mid-height section. Second, even in a purely two-dimensional flow, the time-averaged velocity field is not a sufficient predictor of the mean drag force. The instantaneous pressure forces acting on the flag depend on the coupled state of the flow and the flag deformation: a vortex passing near a nearly flat flag produces little net force, whereas the same vortex at the same location during a strongly deflected configuration acts on a large projected surface and generates a substantial contribution to the drag. The mean force thus reflects correlations between the instantaneous flag shape and the instantaneous flow structure, information that is lost when the velocity field is averaged in time.

In previous work on rectangular flags, we studied the effect of aspect ratio (H/L) on the circulation of the vortices in the wake at the flag mid-height (Raynaud & Mulleners, 2026). We showed that the non-dimensional circulation is constant when scaled with the ratio of the flag area over its perimeter or the square root of area. Here, we further investigate the relevant length scale to characterise the effect of taper ratio on the flow topology and circulation in the wake of tapered flags. In fig. 4a, we show the evolution of the circulation flux through the vertical line located at $x = 1.5L$ in the wake of the flag, indicated by the dotted line in the vorticity snapshots in fig. 4b-d. We estimate the shed circulation from the phase-averaged vorticity fields as

$$\Gamma(t) = \int_{0}^{t} \int_{y=-L}^{L} u(\tau)\omega(\tau)\,\mathrm{d}y\,\mathrm{d}\tau \quad . \qquad (3)$$

Negative vorticity shed from the tip of the flag when flapping upwards is convected downstream past the $x = 1.5L$ line where the circulation flux is computed. Each flapping cycle, a shear layer of negative vorticity is released from the flap tip. Most of the circulation is released in approximately $0.1T$ (between $t/T \approx 0.15$ and $t/T \approx 0.25$ in fig. 4a). The start of each cycle, $t = 0$, is defined as the instant at which the circulation flux through $x = 1.5L$ transitions from positive to negative vorticity. The phase origin is adjusted independently for each case to satisfy this condition. The snapshots of vorticity displayed in fig. 4b-d correspond to three instants of the circulation build-up, identified by the markers in fig. 4a. In snapshot fig. 4b, the negative vorticity has been shed from the tip of the flag but has not reached the integration line yet, and the circulation is close to $\Gamma = 0$. In snapshot fig. 4c, the vortex of negative vorticity is at the precise location of the integration line, which corresponds perfectly to the middle of the circulation slope ($t/T \approx 0.2$ in fig. 4a). In snapshot fig. 4d, all negative vorticity has passed the integration line and the positive vorticity is approaching. For $t/T > 0.5$, little to no negative vorticity is convected past $x = 1.5L$ and the estimated circulation reaches a plateau (fig. 4a). The temporal evolutions of the circulation for the flags of different taper ratio do not collapse when the circulation is normalised by the free-stream velocity U_∞ and the maximum length of the flag L.

Scaling analysis of flow data from rectangular flags of different aspect ratios have shown that the length L is not the suitable characteristic length to scale the flow quantities (Raynaud & Mulleners, 2026). The ratio of the area over the perimeter $L^* = L(H_0 + H_1)/2P$ is used to scale the wake dynamics behind flat plates (Fernando & Rival, 2016). The square root of the area $\sqrt{L(H_0 + H_1)/2}$ is used to scale circulation, hydrodynamic impulse, and kinetic energy for accelerated polygonal disks (Caverly & Nedić, 2025). Both metrics show a collapse of the temporal evolution of the circulation behind rectangular flags. In the current study, all trapezoidal flags have the same area. We choose to define the perimeter as the external perimeter, the sum of the lengths of the flag sides that are not attached to the pole. This aims to account for differences in spanwise height in flags of different tapering and correct spanwise variations in the estimated fluid loading. We expect the tapering to interfere with the three-dimensional geometry of the vortex tube. The external perimeter is an estimation of the length of this vortex tube. The normalisation of the maximum circulation with the maximum length and the ratio of the external perimeter to area are shown in fig. 4e-f. We do not observe an improved scaling of the maximum circulation for tapered flags when using the perimeter to area ratio. This suggests that the difference in vortex tube length are not sufficient to account for differences in mean drag and that the local curvature of the vortex tube has an important influence which is not captured by the perimeter to area ratio.

CONCLUSION AND PERSPECTIVES

We investigated the effect of taper ratio on the flapping dynamics, wake topology, and drag of trapezoidal flags. Diverging flags extract up to twice the momentum from the flow compared to converging flags, yet the momentum deficit measured in the mid-plane wake is inconsistent with the measured drag coefficients. This discrepancy highlights the inherently three-dimensional nature of the wake: the spanwise variation in chord length and trailing-edge geometry for tapered flags produces complex vortex structures that cannot be characterised from mid-plane measurements alone. We highlight the fact that the mean drag force reflects correlations between the instantaneous flag deformation and the instantaneous flow structure that are invisible in time-averaged velocity fields. Attempts to collapse the shed circulation using geometric scaling parameters such as the flag length and the perimeter-to-area ratio do not yield a universal scaling, suggesting that the local curvature of the vortex tube plays an important role. These findings motivate future three-dimensional wake measurements to reconstruct the full vortex topology and connect it to the spanwise distribution of fluid loading.

Next steps in this work include scanning stereo-PIV measurements along the height of the flag to reconstruct the wake vortices in three dimensions. This data will aid to understand three-dimensional effects such as the interaction of the three-dimensional geometry of the vortex tube with the flag with various tapering ratios. We also plan to connect the observed variations of the wake topology along the height of the flag to the spanwise variations in the fluid loading. Based on the spanwise-distribution of the fluid loading, we aim to predict the forces using a quasi-steady Prandtl lifting line approach.

REFERENCES

Caverly, Dylan & Nedić, Jovan 2025 Invariant scaling of impulsively started polygonal disks. *Journal of Fluid Mechanics* **1010**.

Fernando, John N. & Rival, David E. 2016 Reynolds-number scaling of vortex pinch-off on low-aspect-ratio propulsors. *Journal of Fluid Mechanics* **799**.

Floryan, Daniel, Van Buren, Tyler & Smits, Alexander J 2020 Swimmers' wake structures are not reliable indicators of swimming performance. *Bioinspiration & Biomimetics* **15** (2), 024001.

King, Justin T. & Green, Melissa A. 2023 The influence of trailing edge shape on the wake circulation and time-averaged wake of bio-inspired pitching panels. *Experiments in Fluids* **64** (6), 116.

Leroy-Calatayud, Pierre, Pezzulla, Matteo, Keiser, Armelle, Mulleners, Karen & Reis, Pedro M. 2022 Tapered foils favor traveling-wave kinematics to enhance the performance of flapping propulsion. *Physical Review Fluids* **7**, 074403.

Pang, Zhen, Jia, Lai-bing & Yin, Xie-zhen 2010 Flutter instability of rectangle and trapezoid flags in uniform flow. *Physics of Fluids* **22** (12), 121701.

Raynaud, Gaétan & Mulleners, Karen 2025 Event-based reconstruction of time-resolved centreline deformation of flapping flags. *Measurement Science and Technology* **36** (4), 045408.

Raynaud, Gaétan & Mulleners, Karen 2026 On the wake and flapping dynamics of different aspect ratio flags. *physics.flu-dyn, arXiv* .

Terrington, S. J., Hourigan, K. & Thompson, M. C. 2020 The generation and conservation of vorticity: deforming interfaces and boundaries in two-dimensional flows. *Journal of Fluid Mechanics* **890**, A5.